IDENTIFICATION OF FAILURE MECHANISMS IN CFRP LAMINATES USING 3D DIGITAL IMAGE CORRELATION

Nora Schorer[1], Markus G. R. Sause[1]

[1]Experimental Physics II, Institute of Physics, University of Augsburg
Universitätsstr. 1, D-86159 Augsburg, Germany
Email: nora.schorer@physik.uni-augsburg.de, web page: http://www.physik.uni-augsburg.de/exp2

Keywords: Digital image correlation, Failure mechanisms, Full field strain measurement, Finite element modelling

ABSTRACT

Digital image correlation is one of the non-contact methods which are increasingly applied to the investigation of deformation behaviour of materials under load. The method provides full field strain measurements and therefore also offers the possibility to detect local strain inhomogeneities. Based on such measurements, the localization and characterization of critical areas in the structural design is possible. Considering carbon fibre reinforced polymers the ultimate strength of a component is limited by the occurrence of material damage on various length scales. Depending on the applied load type, different failure mechanisms may appear which originate from small defects on the microstructural level and grow into complex failure modes on the macroscopic level. Therefore, it is necessary to identify different failure mechanisms and to assess their contribution to ultimate failure. The experimental approach of this work is the detection of artificially introduced defects within a flat composite laminate under tensile load by means of high-resolution 3D digital image correlation. Various defects being representative for failure mechanisms such as fibre failure, inter-fibre failure and delamination are embedded within the test laminates. For validation of the defect shape and location high-resolution X-ray computed tomography is used. For the digital image correlation measurements, the detection limit in terms of the strain resolution and the spatial resolution is assessed. The influence of several experimental parameters to achieve the highest resolution is outlined. The main focus is the visualization of significant strain signatures being caused by the presence of the different artificially introduced defects. To accompany the experimental investigations, finite element modelling is used to calculate the local strain concentration of the embedded artificial defects.

1 INTRODUCTION

The failure behaviour of composite materials shows a high complexity due to the inhomogeneity and anisotropy of the material. The development of different macroscopic failure types leads to a change of the mechanical behaviour and can finally yield ultimate damage. Typical failure mechanism such as fibre breakage, delamination and inter-fibre cracks are well known and have been frequently investigated in recent years [1]. The onset of failure often appears within the composite from inhomogeneities which can act as so-called stress raisers and can come with a broad range of geometries. All these inhomogeneities, such as voids, inclusions and fibre disorientations can initiate cracks on the micro scale and thus induce failure on the macroscale [2], [3].

The mechanical response of a material with local inhomogeneities can be described by the concept of stress concentration using the theory of elasticity [4]. An externally applied load causes a stress distribution within the material which is affected by the presence of geometric discontinuities. A defect such as an internal crack induces a reduction of the effective cross-section of the surrounding material and leads to a so-called stress concentration. Considering the vicinity of the defect the stress concentration decreases with increasing distance to the crack. This description goes back to the definition of stress intensity factors in fracture mechanics [5], [6]. Similar concepts are proposed for

composites, but the exact definition of such stress concentration factors is still a subject of current research due to the anisotropy and the complex microstructure [7].

A relation between stress and strain concentration for linear elastic material behaviour is given by Hooke´s law. Even though fully linear elastic behaviour is not valid in the direct vicinity of the crack tip, there is still a distinct proportionality of stress and strain concentration to be expected.

As a consequence of these two considerations one can conclude that a local strain concentration should occur due to the presence of defects. With respect to the different failure mechanism the changes of local strain concentration will also depend on the type of failure, the size and orientation.

In failure analysis a variety of approaches are developed for computational modelling. According these methods the finite element method (FEM) is a very suitable tool for prediction of failure in composites. For the present purpose it provides the possibility to calculate stress and strain concentrations of internal inhomogeneities [8].

For experimental investigation of stress and strain concentration in solids there is a variety of established experimental methods such as strain gages, stereography, photo elasticity and digital image correlation (DIC) [9], [10].

The present paper describes an experimental study to investigate artificially introduced failure types (defects) in a carbon fibre reinforced polymer (CFRP) laminate. Full field strain measurements are performed by 3D DIC and the strain concentration of the artificial defects are simulated by a numerical approach using finite element method modelling. Position and shape of the artificial defects are evaluated by high-resolution computing tomography (CT). These objectives of this study are the following:

- Demonstrate visibility of strain signature of introduced defects
- Comparison of experimental data to finite element modelling prediction
- Evaluation of the strain concentration as function of size and depth position of defect

This article presents the experimental setup used to measure strain concentration in section 2, followed by a short description of the FEM methodology in section 3. The data reduction strategy used herein is presented in section 4 and discussion of the results is made in section 5.

2 EXPERIMENTS

2.1 Specimen preparation

The experimental work comprises tensile testing of unidirectional laminates containing artificially introduced defects of four sizes and various depth positions which are marked in red colour in Figure 1 with fibre axis in parallel to the y-axis. Specimens were cut from a plate made from Sigrafil CE 1250-230-39 carbon/epoxy prepreg of eight plies which was cured at 130 °C according to the recommendations of the material supplier. Specimens have a nominal thickness of 1.76 mm, a width of 20 mm or 30 mm and a clamping length of 115 mm. Tabs of a length of 40 mm made from glass fibre reinforced polymer are bonded to the specimens (Figure 2).

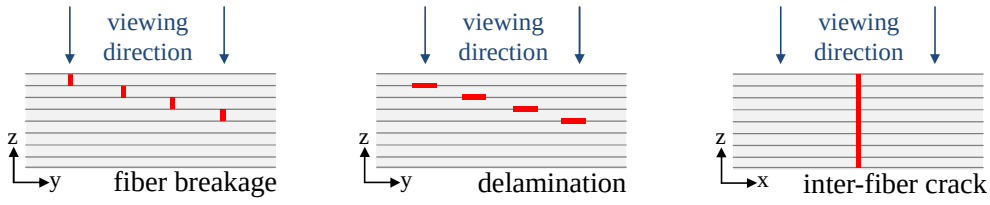

Figure 1: Depth positions of defects within the unidirectional laminate for fibre breakage, delamination and inter-fibre failure

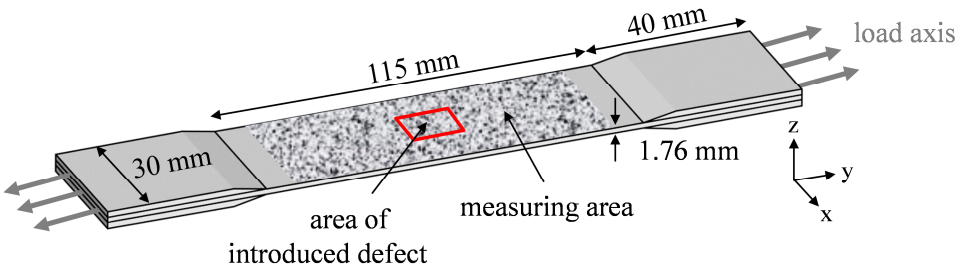

Figure 2: Specimen dimensions for tensile testing with marked measuring area

Three types of failure mechanism such as fibre breakage, delamination and inter-fibre cracks are artificially introduced during the fabrication process.

Fibre breakage is introduced by cutting fibres perpendicular for a certain length spanning the full thickness of one ply. Different cutting lengths of 2.5 mm, 5 mm, 7.5mm and 10 mm are prepared for each ply. Depth positions are chosen from the first ply (surface) down to the fourth ply (below surface). As depicted in Figure 3a the fibre cut can be visualized by a CT measurement to obtain exact information about the geometry of the defect. CT scans with a resolution of 14.29 µm per voxel were made with 2000 images and an X-ray energy of 80 kV and 160 µA using high-resolution computing tomography (phoenix nanotom® m GE). In the present case the fibre cut is slightly disoriented from a straight line in x-direction.

For introduction of an artificial delamination a thin double-layered ETFE foil (Wrightlon®5200) with a foil thickness of 25 µm is welded together at the edges using a hot wire processing technique and is embedded into the laminate. As a consequence the upper and lower part of the foil bag can slide against each other under load while the welded edges prevent the penetration of the surrounding resin during curing of the laminate. Different edge dimensions of quadratic delamination defects (2.5 mm, 5 mm, 7.5mm, 10 mm) are used. The CT image in Figure 3b shows the internal cross-section of the delamination within the laminate. In fibre direction the delamination follows the straight orientation of fibres whereas in x-direction the delamination develops certain waviness.

Inter-fibre cracks in unidirectional laminates are expected to occur throughout the full thickness of the laminate. To introduce inter-fibre cracks two different defect sizes (5 mm and 10 mm) are manufactured by using a PI foil with a thickness of 50 µm (DuPont™Kapton®HN) which is stiffer than PTFE and thus able to withstand the consolidation pressure during the curing process. Nevertheless the PI foil tends to deviate slightly from an exact orientation of 0° in the y-z-plane during the laminate fabrication as can be seen in Figure 3 from the CT image.

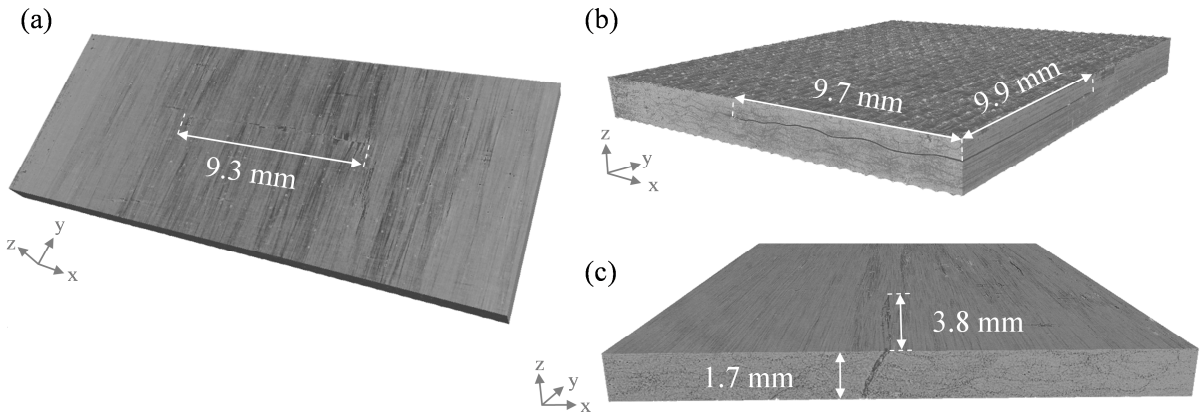

Figure 3: 3D CT images of artificially prepared fibre breakage (a), delamination (b) and an inter-fibre crack (c)

2.2 Measurement setup (mechanical and optical measurements)

All specimens are tested in a universal material testing machine (Z250 Zwick/Roell) under displacement control using 1mm/min velocity. Considering the maximal laminate strength of 1800 MPa provided by the material supplier, specimens were loaded only up to a maximum of 700 MPa to avoid ultimate failure of the specimens.

For the investigation of the deformation behaviour a 3D digital image correlation method is used. Full field strain measurements are made with two cameras using a resolution of 4096 x 3072 pixels and a camera lens with a focal length of 100 mm and a lens speed of f/5.6. After calibration the measurement volume of the DIC system is (55.9 x 41.7 x 24.7) mm^3 for all tests. This yields a resolution of 13.6 µm/px. The images are captured during tensile testing with a frequency rate of 2 Hz using a digital image correlation system (ARAMIS 12M GOM). A speckle pattern which is sprayed on the specimen surface defines the measurement area (cf. Figure 2). For computation of the local strain values the measured images are divided into subsets with the size of (21 x 21) px and an intersection with its neighbouring subsets of approximately 50 %. The shape and position of each subset is compared to a reference image and traced for each subsequent image by a correlation algorithm. Based on the calibration algorithm, for the present setup the image correlation accuracy was evaluated to be 0.04 px. Full-field strain information can be derived from the position and deformation of subsets by calculation of the displacement vectors of the undeformed state with respect to the deformed state. For our measurements, the strain tensor of each subset is obtained from the displacement vectors of the 3x3 subset neighbourhood.

3 FINITE ELEMENT MODELLING

For the finite element method modelling the “structural mechanics module” of the commercial software package Comsol Multiphysics is used. A full 3D representation of the experimentally used geometries is implemented and discretized by a mesh using linear order shape functions and a maximum edge length of 0.5 mm with substantial mesh refinement down to 10 µm when approaching the crack tips. The individual plies of the test specimen are chosen as homogenous unidirectional material with an orientation in accordance with the experimental configuration. The reinforcement sections are modelled as stacking sequence of $[+45/-45/0]_{sym}$. For modelling of the strain concentration, a stationary tensile load is applied as force at the top and bottom surfaces of the reinforcements on one end of the specimen in accordance with the experimental configuration. The opposite side of the specimen uses fixed displacement conditions at the top and bottom surface of the reinforcements. All geometric dimensions of the tensile specimens are matched to the experimental values, with their nominal dimensions shown in Figure 2. The material data used is reported in Table 1 and was validated to yield accurate full-field strain predictions up to 700 MPa stress and is thus used for all further computations. Modelling of the embedded defects makes use of a thin elastic layer boundary condition applied on an internal boundary of dimensions and orientations corresponding to the experimentally used sizes. For fibre breakage, the thin elastic layer is set fully decoupled, i.e. all stiffness values are set to zero. For modelling of delamination, the out-of-plane stiffness is chosen to correspond to the elastic properties of ETFE, while in-plane stiffness is set to zero. For matrix crack modelling, the out-of-plane and in-plane stiffness is set to elastic properties of PI.

	Density [kg/m³]	Poisson-Ratio	Elasticity Constants [GPa]
Sigrafil CE 1250-230-39	1500	-	C_{11}=131.0 C_{12}= C_{13}=3.7 C_{22}= C_{33}=8.1 C_{23}=3.1 C_{44}=2.1 C_{55}= C_{66}= 6.1
ETFE	1750	0.33	1.5
PI	1430	0.40	3.3

Table 1: Material properties used for FEM modelling.

4 DATA EVALUATION

4.1 Data reduction

The evaluation of the measurements has its focus on the evaluation of local strain concentrations, i.e. differences in strain values in the region of introduced defects relative to the global strain field. This strain difference for a certain load level *i* can be described by:

$$\Delta\varepsilon_i = \bar{\varepsilon}_{\text{defect}} - \bar{\varepsilon}_{\text{global}} \tag{1}$$

using

$$\bar{\varepsilon}_{\text{defect}} = \frac{1}{m} \sum_{j=1}^{m} \varepsilon_j \quad \text{and} \quad \bar{\varepsilon}_{\text{global}} = \frac{1}{n} \sum_{k=1}^{n} \varepsilon_k \tag{2}$$

where *n* is the total amount of subsets evaluated in the global strain field. The global strain field is evaluated from the measurement area excluding the area of the defect as seen in Figure 4a. The value *m* is the number of single evaluation points of strain concentration in the region of the defect. For our measurements *m*=5 measurement points were evaluated at spots of highest strain values as seen in Figure 4b. The evaluation of Δε yields a linear relation to the stress level σ (Figure 4c). Thus normalization of Δε by the corresponding load level σ in the range between 250 - 500 MPa provides a mean value including standard deviation expressed as delta strain per stress for the investigated defect.

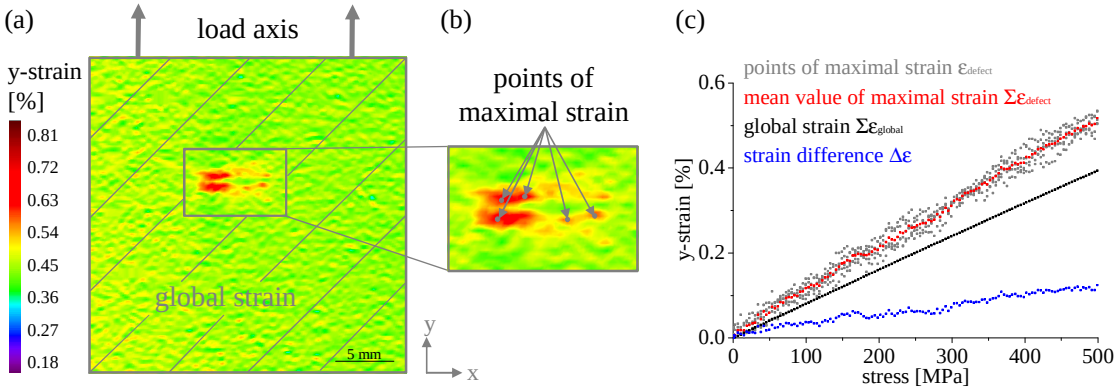

Figure 4: Data reduction routine for DIC measurement (a) selecting points of maximal strain (b) and their evaluation as function of stress (c).

4.2 Influence of subset parameters

In order to discuss strain concentration effects, a brief assessment of system accuracy shall be provided first. The spatial resolution of the measured strain field is determined by the camera resolution and the subset parameters. Whereas the camera resolution first of all depends on the resolution of the camera sensor and the measurement distance to the object, the spatial resolution of the strain field is also the result of the size and intersection of the chosen subsets and thus will add to the ability to detect smaller defects.

To demonstrate this impact, tensile tests of a specimen with an artificial fibre cut are performed with camera lenses of a focal length of 50 mm and 100 mm, respectively. The strain field is calculated using different subset sizes and subset intersection and the data reduction of 4.1 is applied. In Figure 5 the evaluation results of $\bar{\varepsilon}_{\text{global}}$ and $\bar{\varepsilon}_{\text{defect}}$ using *m*=5 strain values in the vicinity of an embedded fibre crack with the length of 7.5 mm are shown. For this investigation two equivalent strain measurements with a 50 mm and a 100 mm camera lens are used. The global strain is 0.45 % at a load level of 568 MPa.

The absolute values of the global strain field remain almost unchanged as function of subset intersection, subset size and camera lens (cf. Figure 5a and Figure 5b). However, the decrease of subset size gives rise to increasing uncertainty in $\bar{\varepsilon}_{\text{global}}$. In contrast, the influence of these parameters

is not found negligible for the values of $\bar{\varepsilon}_{defect}$. Considering the subset intersection shown in Figure 5a, $\bar{\varepsilon}_{defect}$ increases with higher subset intersection due to the higher spatial resolution given by the same 3x3 neighbourhood when increasing the intersection. Thus, to obtain a reasonable measure of $\Delta\varepsilon$ without exceeding the computational resources by the increasing number of subsets, an intersection of approximately 50 % is chosen in the following. Due to the increase of uncertainty in the measurement of $\bar{\varepsilon}_{global}$ the subset size is set to 0.286 x 0.286 mm (21 x 21 pixels) to achieving a good balance between spatial resolution and noise level.

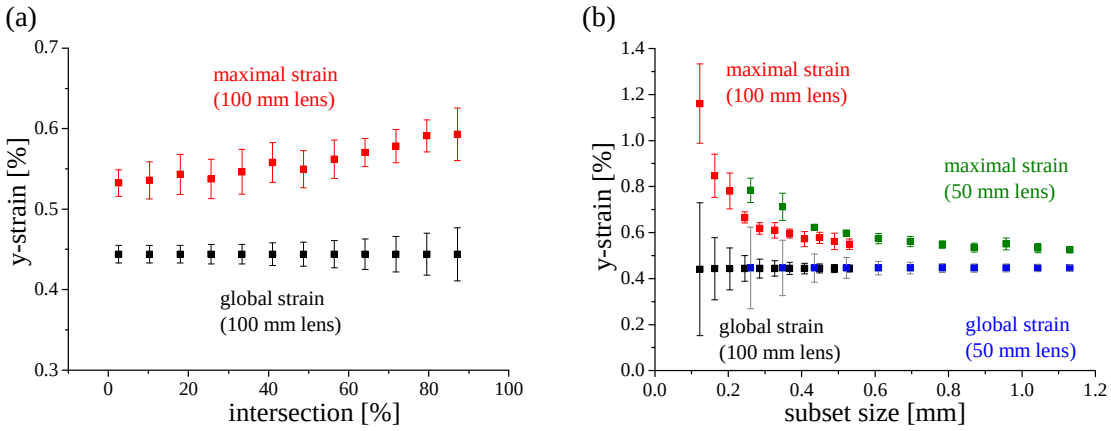

Figure 5: Influence of subset intersection (a) and subset size (b) on absolute strain level.

5 RESULTS AND DISCUSSION

Considering the embedded fibre cuts all defects show significant strain signatures under load which can be well distinguished from the global strain field. As an example Figure 6a shows a full field strain measurement of a fibre cut with a length of 7.5 mm in the second ply at a stress level of 569 MPa. The strain component parallel to the load axis is used as false colour information. For this exemplary image the subsets are chosen to have a size of (25 x 25) px with an intersection of 48%. The dashed line indicates the position of the fibre cut. In the surrounding area an increased strain value is clearly observable. Using the geometry of the fibre cut, the strain field at the corresponding load level is computed by finite element modelling (Figure 6b). In direct comparison to the experimental results a good agreement is achieved in terms of the absolute values and the strain distribution in the local area of the defect. Whereas the computation shows a perfectly homogeneous global strain field, the experimental measurement is affected by noise which originates from inhomogeneities of the material on the surface and from the strain measurement using a speckle pattern itself. Differences in strain values which can be seen on the left end of the fibre cut may originate from imperfect orientation of the fibre cut inside the laminate. Additionally, overlaps and warping of the fibres at the edges of the cut can also contribute to inhomogeneities of the strain field.

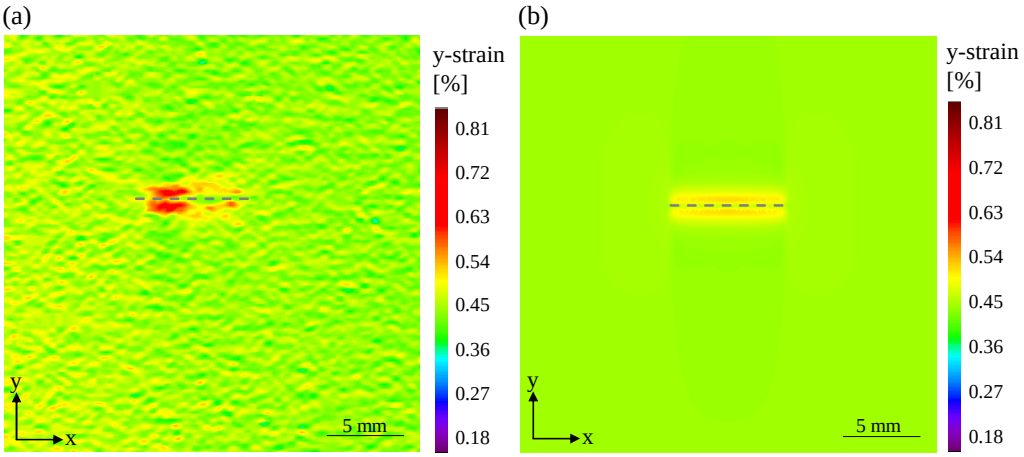

Figure 6: Full field strain measurement of an artificial fibre breakage of 7.5 mm size at the second ply below the surface at 569 MPa (a) and corresponding finite element modelling (b).

A typical measurement result of an embedded delamination is shown in Figure 7a. The strain component in parallel to the load direction is shown as false colour scale at a stress level of 695 MPa. The dashed line refers to a quadratic delamination with the size of 100 mm² at the depth position between the first and the second ply. For edge lengths of 10 mm and 7.5 mm, strain signatures could be distinguished down to a depth between the third and the fourth ply. For the sizes 5 mm and 2.5 mm only delamination between the first and the second ply were found to be visible. Compared to fibre breakage the strain signatures of the embedded delamination show less $\Delta\varepsilon$ in the area of the defect. This is due to the fact that in laminates, fibres predominantly carry the load and therefore a fibre breakage causes a stronger stiffness reduction of the laminate when compared to a delamination of the same spatial dimensions.

As shown in Figure 7a strain signatures occur within the area directly above the delamination as well as outside the indicated area all along the y-axis. The corresponding modelling approach takes into account the waviness of the delamination and leads to very similar strain signatures (Figure 7b) as for the measurement. In contrast to the computation the experimental strain field has an inhomogeneous strain distribution that results from the material structure and the strain measurement by DIC as discussed above. The main difference is caused by the periodic waviness of the modelled delamination, which is not expected to be fully periodic for the experiment. This may also explain the locally increased strain values in the experiment compared to the values found for the modelling result.

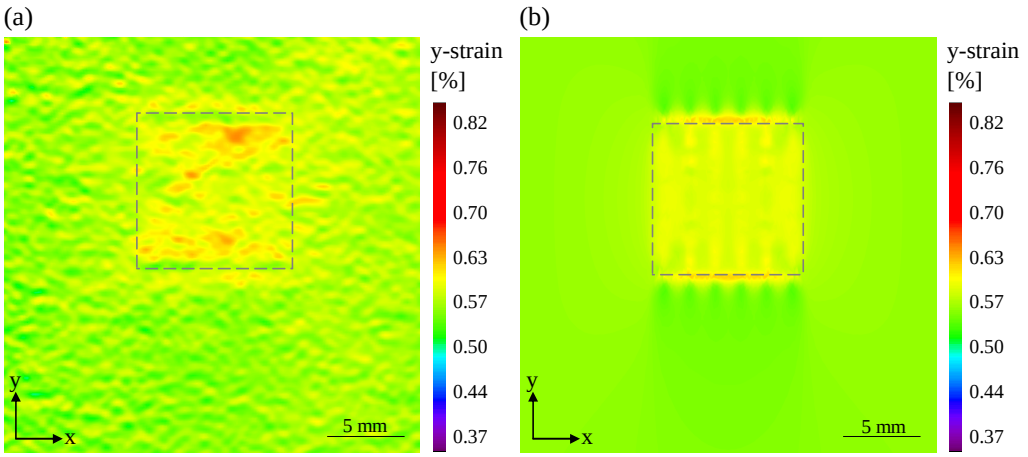

Figure 7: Full field strain measurement of an artificial delamination of 10 mm x 10 mm size between the first and second ply below the surface at 695 MPa (a) and corresponding finite element modelling (b).

For artificial inter-fibre cracks, the Δε values were found to be higher along the x-axis direction. Thus the strain transverse to the load axis is evaluated in the following. In Figure 8a the strain field of an inter-fibre crack with a length of 10 mm is shown at a stress level of 535 MPa. The absolute strain values at the position of the crack indicated as dashed line are lower as in the vicinity of the crack. The reason for this is the local stiffness reduction at the position of the crack due to the embedded PI foil, which causes a higher transverse contraction. The comparison between the experimental and the computed results shows a difference in the spatial strain distribution at the crack position. Here the irregular strain signature in the experimental data may originate from disorientations of the PI foil which can easily tilt around the y-axis and may thus be distorted within the y-z plane.

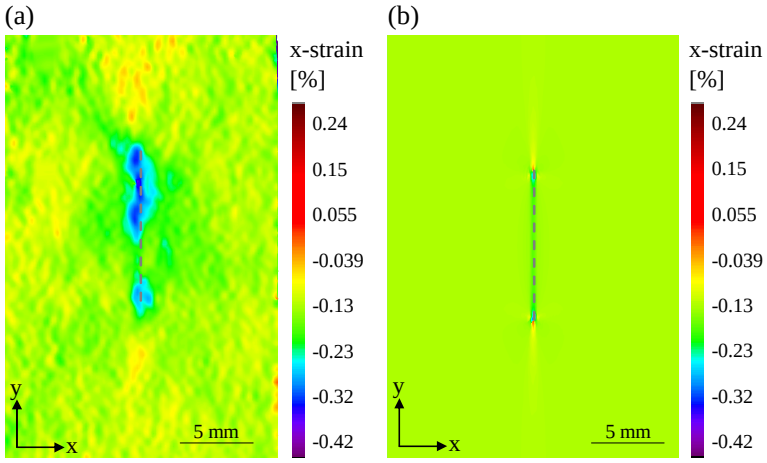

Figure 8: Full field strain measurement of an artificial inter-fibre crack of 10 mm size throughout the whole thickness of the laminate at 535 MPa (a) and corresponding finite element modelling (b).

Following the data reduction strategy presented in section 4.1, the values of $\Delta\varepsilon$ normalized by the stress level are plotted for each defect type as function of the defect size. For the fibre breakage at the surface level $\bar{\varepsilon}_{\mathrm{defect}}$ is determined using all data points at the position of the cut for averaging to avoid incorrect strain values caused by a potentially destroyed speckle pattern, i.e. the value of m was chosen to be in the range of 61 to 325. For indication of the depth position different colours are used in the diagrams.

For direct comparison to the experimental results, the numerical computation values are added to the experimental measurements as well. For the evaluation of the modelling results the absolute value of the strain concentration is obtained by using the output of the maximum value without averaging and is referenced to the strain average by evaluation of the full surface excluding the region of the defect in accordance with the experimental procedure.

The strain concentration of fibre breakage is shown Figure 9. Fibre cuts on the surface level show nearly the same strain concentration regardless of the geometric dimensions. For all fibre cuts within the laminate there is a decrease of strain concentration with decreasing defect size because the remaining intact fibres surrounding the crack can easier compensate the missing cross-section. Due to the existence of the defect a strain gradient occurs within the volume. As a consequence, the strain concentration which is measured at the surface level is lower for defects with higher distance to the surface because of the shielding effect given by the presence of the other plies above the defect. Compared to the results of the modelling the experimental values show good agreement taking into account the measurement errors and the uncertainty of the defect position and orientation. Thus it may be speculated, that the strain concentration of the fibre cut with 2.5 mm length has a deviation of orientation and position and therefore shows a distinct difference to the trend described by the modelling results.

For delamination failure the experimental and modelling results presented in Figure 10 show generally lower strain concentration values as discussed before. Considering the size and depth

position between two plies there is a similar trend as for fibre cuts in the volume whereas the values of delamination failure is generally lower than for fibre cuts.

Figure 11 shows the strain concentration of inter-fibre cracks as function of the size and orientation to the z-direction, i.e. a perfectly oriented inter-fibre crack has an orientation of 0°. As trend the strain concentrations decrease with an angle of 0° to 90°. A 90° oriented inter-fibre crack would by concept be identical to a delamination in the middle plane of the laminate. Up to 45° the strain concentration is thus decreasing with decreasing defect size and for angles between 0° and 45° there is an inverted trend, owing to a sinusoidal behaviour as function of orientation angle.

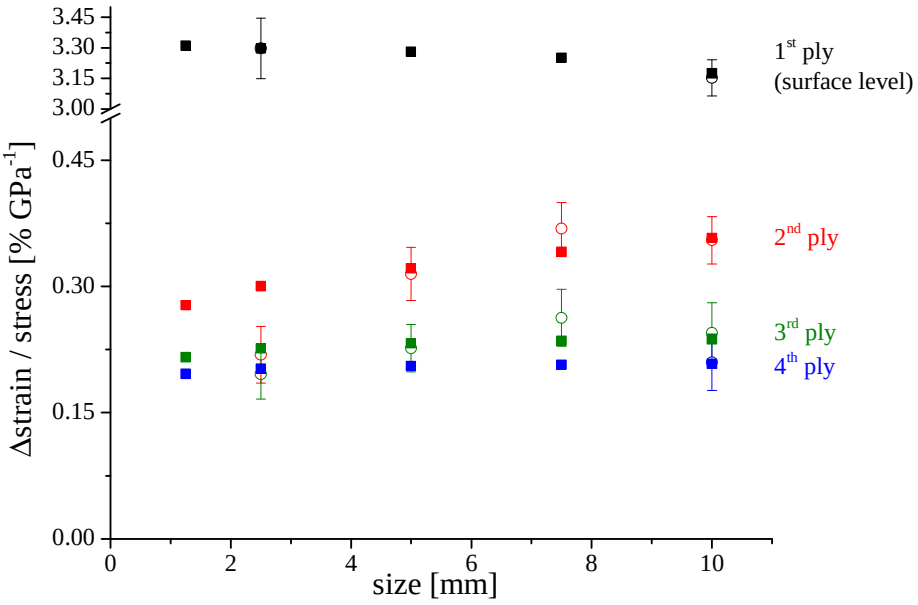

Figure 9: Evaluation of strain concentration per external stress in GPa of artificially introduced fibre breakage as function of defect size for different depth positions.

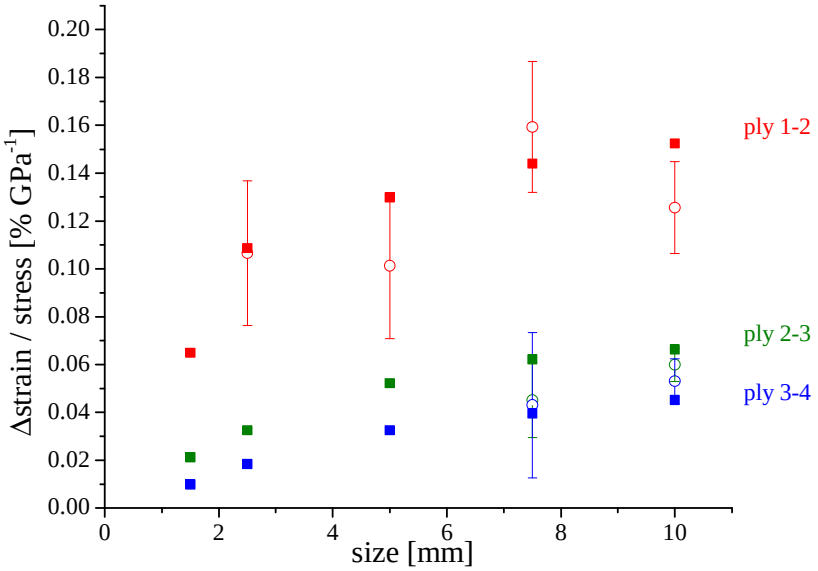

Figure 10: Evaluation of strain concentration per external stress in GPa of artificially introduced delamination defects as function of defect size for different depth positions below surface.

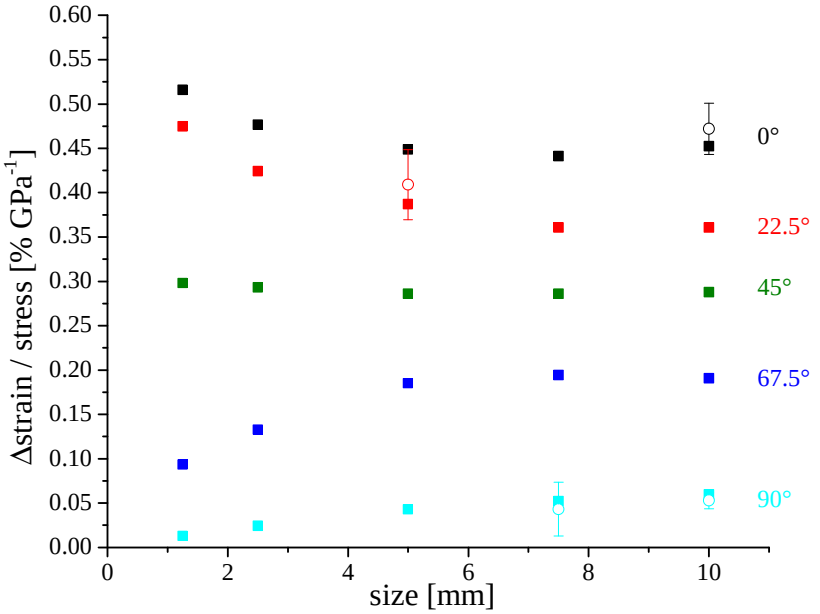

Figure 11: Evaluation of strain concentration per external stress in GPa of an artificially introduced inter-fibre crack as function of defect size for different orientation angles.

6 CONCLUSIONS

The present study demonstrates the possibility to measure a significant strain concentration of artificially introduced defects such as fibre breakage, delamination failure and inter-fibre cracks in unidirectional CFRP laminates by means of 3D DIC under tensile load. Full field strain measurements show a characteristic strain signature which indicates the type of defect. Furthermore, a finite element modelling approach was developed and validated for the used material. The absolute values of strain concentration in the vicinity of defects are obtained by a stable data reduction routine. The computed strain values were found to show high agreement with the measurement results.

Regarding the different types of failure it is found that for fibre cuts and delamination failure the strain components axial to the load axis show the highest visible strain concentration values whereas the strain concentration of inter-fibre cracks is apparently better visible for the strain components transversal to the load axis.

Examining the influence of different defect sizes and depth positions different tendencies with respect to the strain concentrations are observed. While fibre cuts on the surface level show nearly the same strain concentration for different sizes there is a trend of decreasing strain with decreasing size and distance to the surface for fibre cuts located in the volume. Delamination at the interface of two plies obey the same trend for decreasing size and distance to the surface but the strain concentration is generally lower as obtained for fibre cuts. The strain concentration evaluated for inter-fibre cracks in terms of transversal contraction shows a significant dependency on the orientation of the crack.

Based on these first investigations the use of 3D DIC seems a promising technique to study the failure behaviour of composite laminates and to assess the occurrence of different failure types. Further investigations will focus on the possibilities to securely distinguish strain signatures from the background noise and to assess the system limits with respect to defect sizes and defect depths.

REFERENCES

[1] E. S. Greenhalgh, *Failure analysis and fractography of polymer composites*, Woodhead Publishing Limited, Cambridge, 2009

[2] H. Schürmann, *Konstruieren mit Faser-Kunststoff-Verbunden*, Springer, Berlin, 2007.

[3] F. L. Matthews und R. D. Rawlings, *Composite Materials: Engineering and Science*, Woodhead Publishing Limited, Cambridge, 1999

[4] J. Timoshenko und S. Goodier, *Theory of Elasticity*, McGraw-Hill Book Company, New York, 1970

[5] G. Irwin, Analysis of stresses and strains near the end of a crack traversing a plate, *Journal of Applied Mechanics*, 24, 1957, pp. 361-364

[6] H. P. Tada, C. Paris und G. R. Irwin, *The Stress Analysis of Cracks Handboolk*, 2nd ed., Paris Productions Inc., St. Louis, Missouri, 1985

[7] V. Kushch, I. Sevostianov und L. Mishnaevsky, Stress concentration and effective stiffness of aligned fiber reinforced, *International Journal of Solids and Structures*, **45**, 2008, pp. 5103–5117 (doi:10.1016/j.ijsolstr.2008.05.009)

[8] T. E. Tay, G. Liu, V. B. C. Tan, X. S. Sun und D. C. Pham, Progressive Failure Analysis of Composites, *Journal of Composite Materials*, **42**, 2008, pp. 1921-1966 (doi: 10.1177/0021998308093912)

[9] K. Rastogi und E. Hack, *Optical Methods for Solid Mechanics: A Full-Field Approach*, Wiley-VCH, Weinheim, 2012

[10] M. A. Sutton, J.-J. Orteu und H. W. Schreier, *Image Correlation for Shape, Motion and Deformation Measurements*, Spinger, New York, 2009